Metal–organic framework nanoparticles for arsenic trioxide drug delivery

Romy Ettlinger, Marthe Sönksen, Monika Graf, Natalia Moreno, Dmytro Denysenko, Dirk Volkmer, Kornelius Kerl, Hana Bunzen

Angaben zur Veröffentlichung / Publication details:

Ettlinger, Romy, Marthe Sönksen, Monika Graf, Natalia Moreno, Dmytro Denysenko, Dirk Volkmer, Kornelius Kerl, and Hana Bunzen. 2018. "Metal–organic framework nanoparticles for arsenic trioxide drug delivery." *Journal of Materials Chemistry B* 6 (40): 6481–89. https://doi.org/10.1039/c8tb01899e.

Metal–organic framework nanoparticles for arsenic trioxide drug delivery†

Romy Ettlinger,[a] Marthe Sönksen,[b] Monika Graf,[b] Natalia Moreno,[b] Dmytro Denysenko,‡[a] Dirk Volkmer,[a] Kornelius Kerl[b] and Hana Bunzen *[a]

Arsenic trioxide is a double-edged sword: On the one hand it is known as a poison, on the other hand it is used as an anticancer drug. Though effective in the treatment of leukaemia, arsenic trioxide has not been able to be introduced into the treatment of solid tumour entities yet due to its dose-limiting toxicity. However, different *in vitro* and *in vivo* studies revealed arsenic trioxide to be a potent agent against different solid tumour entities, including atypical teratoid rhabdoid tumours (ATRT), a paediatric brain tumour entity with a very poor prognosis. To improve the pharmacokinetics and therapeutic efficacy of arsenic trioxide and to reduce its toxic side effects, we propose to use a metal–organic framework (MOF) as a drug carrier material. Herein we report on using a MOF called MFU-4l (Metal–Organic Framework Ulm University), consisting of Zn(II) ions and bis(1*H*-1,2,3-triazolo[4,5-*b*],[4′,5′-*i*])dibenzo[1,4]dioxin ligands, to deliver arsenic trioxide in a form of dihydrogen arsenite anions. The $H_2AsO_3^-$ anions were introduced to the MOF in a nanoparticle formulation *via* a postsynthetic side ligand exchange. The prepared material was characterised by IR, TGA, XRPD, SEM-EDX, TEM, DLS, ICP-OES and adsorption analysis. The drug release studies at different pH values were carried out as well as cytotoxicity tests with different ATRT cell lines and non-tumorous-control cell lines. The MOF-based material was shown to be a promising candidate for arsenic trioxide drug delivery.

Introduction

Although arsenic trioxide has been reportedly used as a drug in traditional Chinese medicine, it is rather known as the "king of poisons" with a lethal dose value (LD_{50}) as low as 15 mg kg^{-1} (rat, oral).[1] In 2000 it received approval from the FDA (US Food and Drug Administration) for the treatment of refractory or relapsed acute promyelocytic leukaemia (APL)[2] and in 2016, this approval was enlarged to the treatment of newly diagnosed APL by the EMA (European Medicines Agency).[3] The promising results of arsenic trioxide in leukaemia treatment lead to an increased interest in translating the therapeutic effects into the treatment of solid tumours. We recently reported on using arsenic trioxide as a promising drug for the treatment of highly aggressive atypical teratoid rhabdoid tumours (ATRT).[4] ATRT is a brain tumour entity occurring in very young children under the age of three years.[5] Due to the poor prognosis of ATRT,[6] new therapeutic approaches such as the utilization of arsenic trioxide are urgently needed. Unfortunately, the promising pre-clinical results of arsenic trioxide as a therapeutic agent for solid tumours have not been successfully transferred into the treatment of patients yet.[7] One possible explanation is the insufficient enrichment of arsenic trioxide in the tumour tissue.[2,8] However, due to its severe systemic side effects, a mere increase in dosage is not be feasible. To extend the possible medical applications of arsenic trioxide, the utilization of nanocarriers seems to be a promising strategy. Drug delivery *via* nanocarriers offer several advantages over traditional drug distribution pathways: more specific drug targeting and delivery, reduction of the dosing frequency as well as the toxicity effects of the drug, while maintaining therapeutic effects.[9] Despite all these benefits, drug delivery *via* nanocarriers remains challenging. Up to now only few examples of nanocarriers for delivery of arsenic trioxide have been reported in literature.[10] Herein we would like to introduce the application of a metal–organic framework (MOF) as a nanocarrier material for the delivery of arsenic(III) species.

MOFs are crystalline porous coordination polymers consisting of inorganic metal ions (or clusters) and organic ligands. They exhibit outstanding properties including high internal surface area and chemical versatility.[11,12] They have been

[a] *Chair of Solid State and Materials Chemistry, Institute of Physics, University of Augsburg, Universitätsstraße 1, D-86159 Augsburg, Germany. E-mail: hana.bunzen@physik.uni-augsburg.de*

[b] *University Childreńs Hospital Muenster, Pediatric Hematology and Oncology, Albert-Schweitzer-Campus 1, D-48149 Muenster, Germany*

† Electronic supplementary information (ESI) available: Characterization of MFU-4l, MFU-4l-OAs(OH)$_2$ and PEG@MFU-4l-OAs(OH)$_2$, computational modelling, drug release and MOF stability studies and cytotoxicity studies. See DOI: 10.1039/c8tb01899e

‡ Passed away in June 2018.

shown to be promising materials for various applications including gas storage and separation,[13,14] catalysis,[15,16] sensing[17,18] and many others.[19] Recently, their particle size could be scaled down to the nanoregime, which opened up new application possibilities of these materials, in particular in medicine, for instance, as drug delivery vehicles.[20–23] In the majority of the already published reports, the drug molecules have been captured inside the pores *via* weak non-covalent interactions. Therefore, upon administration, the drug has been simply released from the material *via* diffusion, and thus controlled drug release has not been achieved efficiently.[24] However, having a control over the drug release is crucial, and especially when administrating toxic drugs such as arsenic trioxide. Therefore, herein we suggest an alternative approach which is similar to the reported strategies used to bind cationic drugs[25] or organic drugs containing suitable functional groups (COOH, phosphates *etc.*)[26,27] onto metal sites of MOFs. We propose to use a MOF which can form a coordinate bond to the arsenic(III) species, and thus bind the drug in a defined and controlled manner. For this purpose, we selected a MOF called MFU-4l (Metal–Organic Framework Ulm University) recently reported by us.[28]

MFU-4l consists of Zn(II) ions and bis(1*H*-1,2,3-triazolo[4,5-*b*],[4′,5′-*i*])dibenzo[1,4]dioxin (H_2-BTDD) as a ligand (Scheme 1). The secondary building unit, $[Zn^{o}Zn^{t}_{4}Cl_{4}(ligand)_{6}]$, is formed by one zinc ion in an octahedral coordination (Zn^{o}) linked to six N-donor atoms of six different ligands, and by four peripheral zinc ions in a tetrahedral coordination (Zn^{t}), each of them linked to three N-donor atoms of three different ligands. Charge compensation is achieved by negatively charged chloride ligands. It has been shown previously that the chloride side ligands could be postsynthetically exchanged to various molecules such as nitric oxide and nitrogen dioxide.[29,30] Herein we studied the exchange of the chloride anion for anionic arsenic(III) species and the application of the material as an arsenic trioxide nanocarrier for cancer treatment.

Results and discussion

MFU-4l nanoparticle synthesis

Intending to use a MOF as a drug carrier material in cancer therapy, scaling down its particle size to nanoregime is crucial. Herein we synthetized the MFU-4l nanoparticles by applying synthesis procedures recently reported for a structurally related MOF called MFU-4.[31] In comparison to the original synthesis,[28] the reaction time was shortened from 18 h to 30 min, the reaction temperature was lowered from 145 °C to 80 °C and an DMF–ethanol solvent mixture (1 : 1) was used instead of pure DMF. The final product was obtained as an off-white powder in a very high yield (98%). Product crystallinity and phase purity were confirmed by XRPD measurement (Fig. 1b), which revealed a diffractogram comparable to the one simulated. To confirm the formation of nanoparticles, TEM micrographs and DLS measurements were recorded verifying the crystal sizes being around 100 nm (Fig. S1 and Table S1, ESI†).

Drug loading

To deliver the selected drug (arsenic trioxide) in a safe and controlled fashion, we proposed to bind it to the carrier material *via* coordinate bond in a form of an anion. Firstly, arsenic trioxide (1 eq.) was mixed with tetramethylammonium hydroxide (1 eq.) in methanol to prepare tetramethylammoniumdihydrogen

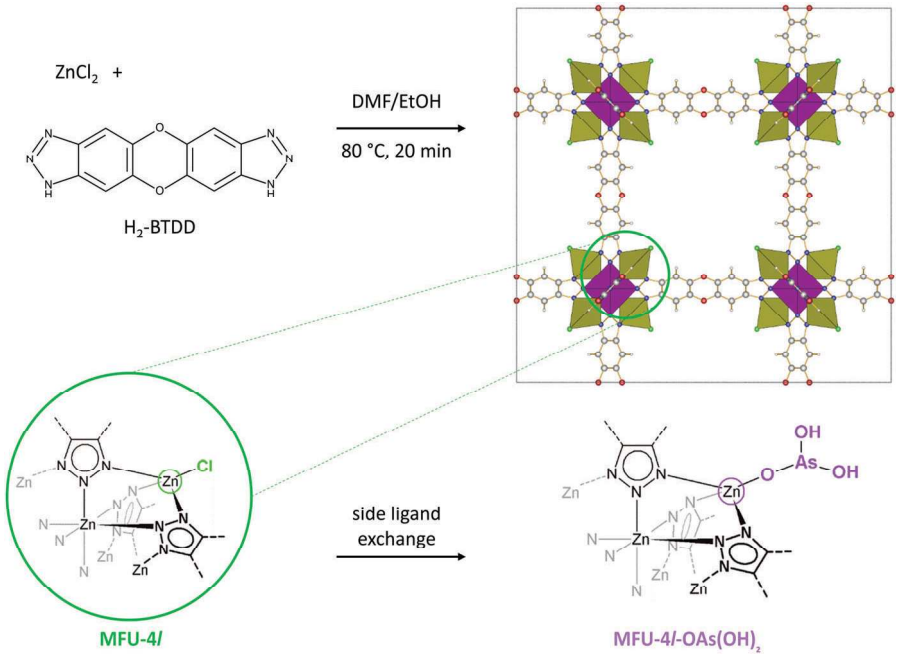

Scheme 1 Crystal structure of MFU-4l featuring the coordination environment of the zinc ions, and the proposed side ligand exchange of the chloride anion to a dihydrogen arsenite anion to form MFU-4l-OAs(OH)$_2$.

arsenite {[$(CH_3)_4N$]H_2AsO_3}. Secondly, the exchange of the chloride side ligand in the structure of MFU-4l was carried out. As-synthetized MFU-4l nanoparticles were kept in a methanolic solution of {[$(CH_3)_4N$]H_2AsO_3} at room temperature overnight. After that, the particles were collected by centrifugation, washed with methanol and dried under ambient pressure at 100 °C (to remove any residual solvent molecules from the pores). To characterise and to quantify the loading of the As(III) species to the MFU-4l carrier material, different analytical methods including FTIR spectroscopy, EDX spectroscopy, ICP-OES analysis, argon adsorption measurements and XRPD analysis were used.

The application of FTIR spectroscopy turned out to be a very useful method to verify and to qualify the side ligand exchange in the MFU-4l structure. In the IR spectrum new bands were observed in the range from 800 to 500 cm^{-1} (Fig. 3 and Fig. S9, ESI†). According to literature,[32] the bands at 570, 610 and 790 cm^{-1} correspond to the symmetric and asymmetric mode of $As(OH)_2$ and As–O stretching vibrations. This was further confirmed by a computational simulation of IR spectra of various As(III) anionic species (Table S3, Fig. S7 and S8, ESI†). Both computational modelling and IR spectroscopy confirmed that the chloride side ligands in MFU-4l were successfully exchanged to the $H_2AsO_3^-$ anions to form MFU-4l-$OAs(OH)_2$ (Scheme 1).

To quantify the extent of the side ligand exchange, EDX spectroscopy and ICP-OES analysis were carried out (Table 1). Based on the results, more than 86% of the chloride ions were exchanged to the $H_2AsO_3^-$ anions. Due to the exchange of the chloride with $H_2AsO_3^-$ anions, one would expect a decrease in the specific surface area. Indeed, the adsorption analysis revealed the BET surface area, determined in the range p/p_0 = 0.06–0.1, as high as 2755 $m^2\ g^{-1}$ which was a significantly lower than the BET surface area of the same material before the side ligand exchange (Table 1). This value is in good agreement with the calculated specific surface area of 2562 $m^2\ g^{-1}$ from the crystal model of MFU-4l-$OAs(OH)_2$ (shown in Fig. 1a) using the Poreblazer software.[33] The argon adsorption isotherms for both samples revealed the type I sorption behaviour, which is characteristic for microporous solids (Fig. S2, ESI†). The maximum uptake achieved at 77 K and p/p_0 = 0.99 was 1260 $cm^3\ g^{-1}$ for MFU-4l and 1190 $cm^3\ g^{-1}$ for MFU-4l-$OAs(OH)_2$, which corresponds to a total pore volume of 1.32 $cm^3\ g^{-1}$ and 1.11 $cm^3\ g^{-1}$, respectively. To evaluate the pore size distribution, the argon adsorption isotherm sampled for MFU-4l-$OAs(OH)_2$ at 77 K was analysed using non-local density functional theory (NLDFT)[34] implementing a carbon equilibrium transition kernel for argon adsorption based on a slit-pore model.[35] The pore size distribution calculated by fitting the adsorption data revealed micropores in the range of 11–18 Å with maxima at 13 and 16 Å (Fig. S3, ESI†). The range found for MFU-4l-$OAs(OH)_2$ was slightly lower in comparison to the data reported for MFU-4l (11–20 Å)[28] which was, however, expected. The introduction of As(III) anionic ligands did not only influence the specific surface area, but also the symmetry of the crystal structure proven by the XRPD measurement (Fig. 1b). The details of the crystal structure

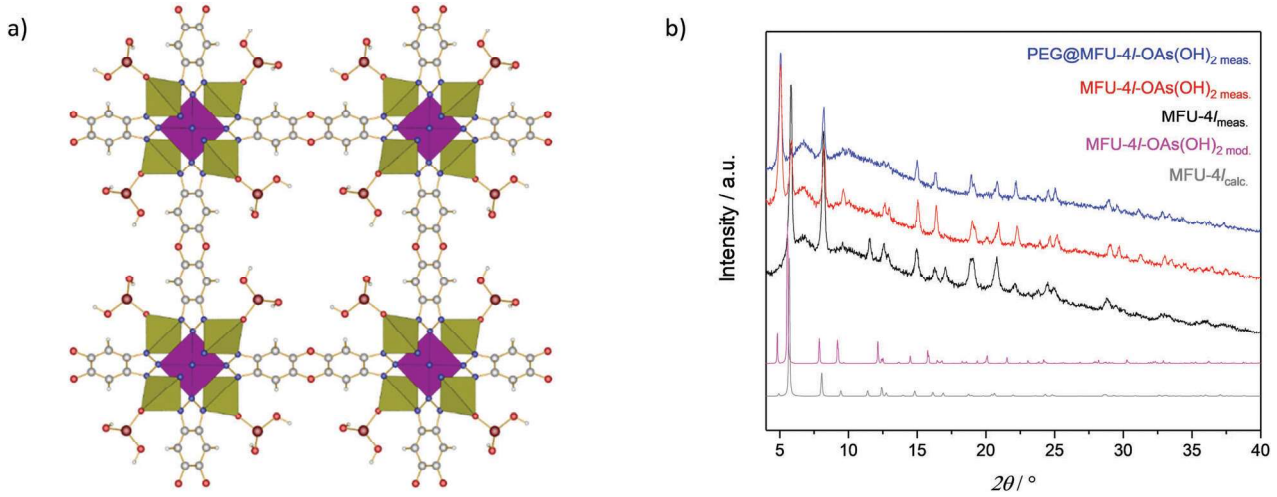

Fig. 1 Modelled crystal structure of MFU-4l-$OAs(OH)_2$ ((a) see ESI† for computational details) and comparison of the calculated XRPD patterns of MFU-4l (grey) and MFU-4l-$OAs(OH)_2$ (pink), and measured XRPD patterns of MFU-4l (black), MFU-4l-$OAs(OH)_2$ (red) and PEG@MFU-4l-$OAs(OH)_2$ (blue) (b).

Table 1 Results of EDX spectroscopy, ICP-OES and adsorption analysis of the side ligand exchange in MFU-4l

Analysis	MFU-4l	MFU-4l-$OAs(OH)_2$	PEG@MFU-4l-$OAs(OH)_2$
EDX, n(Zn) : n(As) : n(Cl)	5 : 0 : 4	5 : 3.8 : 0.2	5 : 3.7 : 0.1
ICP-OES, n(Zn) : n(As)	5 : 0 : —	5 : 3.44 : —	5 : 3.40 : —
Meas. spec. surface area (Ar, 77 K)	3580 $m^2\ g^{-1}$	2755 $m^2\ g^{-1}$	—
Calc. spec. surface area (with Poreblazer[27])	3184 $m^2\ g^{-1}$	2562 $m^2\ g^{-1}$	—

data of MFU-4l and MFU-4l-OAs(OH)$_2$ are summarized in Table S4 and Fig. S10 in ESI.† The thermal stability of MFU-4l-OAs(OH)$_2$, which was studied by variable temperature X-ray powder diffraction and thermogravimetric analysis (Fig. S4 and S5, ESI†), was found to be only slightly lower in comparison to the MFU-4l nanoparticles.

The successful combination of MFU-4l and $H_2AsO_3^-$ represents a novel approach to the nanocarrier design for arsenic trioxide delivery, featuring a definite drug binding and a high drug loading capacity (approximately 0.18 g of As per 1 g of the material).

Coating nanoparticles with polyethylene glycol

To improve the material stability and biocompatibility, MFU-4l-OAs(OH)$_2$ nanoparticles were coated with polyethylene glycol (with an average molecular mass of 6000, PEG 6000), a well-established polymer in the field of drug delivery.[36] The successful coating of the nanoparticles was confirmed by IR spectroscopy. In the FTIR spectrum of the coated sample (Fig. S6, ESI†), the bands at 1290, 1230, 1100, 950 and 840 cm^{-1} corresponding to C–H bending vibrations, O–H and C–O–H stretching vibrations could be detected. Further, the thermogravimetric analysis verified that PEG 6000 was present with approximately 3 wt% (Fig. S5, ESI†). The arsenic content in the coated nanoparticles was determined by EDX spectroscopy and ICP-OES analysis which confirmed that still more than 85% of the chloride ligands were exchanged to arsenic anions (Table 1). Herein we used noncovalent interactions to coat the nanoparticles. Therefore, some of the polymer molecules might be partly included inside the pores. To avoid this, some of the recently reported covalent surface coating methods could be used as an alternative.[21]

Drug release

The arsenic release from MFU-4l-OAs(OH)$_2$ and PEG@MFU-4l-OAs(OH)$_2$ nanoparticles was studied in a phosphate buffered saline at two different pH values, pH 6 and pH 7.4 at 37 °C. After 30 min, 1 h, 4 h, 6 h, 24 h, 72 h and 168 h the amount of arsenic and zinc released into the solution was determined by ICP-OES (Fig. 2, Fig. S11 and Table S5, ESI†).

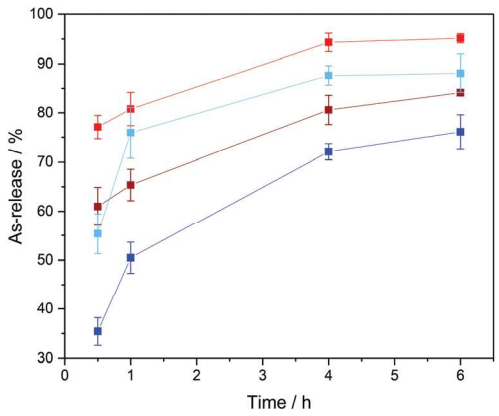

Fig. 2 Arsenic release from MFU-4l-OAs(OH)$_2$ and PEG@MFU-4l-OAs(OH)$_2$ at pH 6 (red, light blue) and pH 7.4 (dark red, dark blue) in a phosphate buffer solution at 37 °C determined by ICP-OES.

The arsenic release from MFU-4l-OAs(OH)$_2$ was quite fast, reaching approximately 75% at pH 6 and 60% at pH 7.4 within the first 30 minutes. After 24 h the release was almost complete with more than 90% for both tested pH values (Table S5, ESI†). For the coated PEG@MFU-4l-OAs(OH)$_2$, the arsenic release was slowed down significantly to 55% at pH 6 and 35% at pH 7.4 within the first 30 minutes. After 24 h, the nearly complete release around 90% was reached at pH 6.0 in comparison to only 80% at pH 7.4 (Table S5, ESI†). These results clearly indicate that the arsenic release from MFU-4l is pH dependent (faster for lower pH value), suggesting that the MOF material could be very useful in cancer therapy where drug release triggered by lower pH values is desired.[37,38] Additionally, it was demonstrated that coating the nanoparticle surface with PEG could be used as an effective tool to tune the drug release kinetics.

To study the nanocarrier stability, the solid materials used in the drug release studies were collected after 1, 24, 72 and 168 h, and analysed by IR, XRPD and TGA. The FTIR spectroscopy revealed a decrease of the signal intensity of the bands assigned to the arsenic species which was in agreement with the observed drug release. At the same time a new broad band between 1100 and 950 cm^{-1} was observed which could be assigned to HPO_4^{2-} suggesting that the $H_2AsO_3^-$ anions were substituted by the phosphate anions from the buffer solution (Fig. S12–S15, ESI†). Moreover, several additional bands were detected. These bands matched with the bands of the ligand H_2-BTDD indicating partial framework decomposition during the drug release tests. This was especially true for the release studies carried out at pH 6. A similar pH-dependent stability has been observed also for some other Zn-MOFs based on N-donor ligands such as, for instance, ZIF-8.[39] The presence of the free ligand (which is insoluble in aqueous solutions) was further confirmed by TGA (Fig. S16–S19, ESI†). The XRPD measurements of the solids kept at pH 6 showed that the MOF was stable less than 24 h and that zinc cations released from the MOF reacted with the buffer ions to form $Zn_3(PO_4)_2{\cdot}4H_2O$ and $NaZn(PO_4){\cdot}H_2O$ salts (Fig. S20 and S22, ESI†). On the contrary, the framework kept at pH 7.4 was stable for at least 72 h forming $NaZn(PO_4){\cdot}H_2O$ and $Na_6Zn_6(PO_4){\cdot}8H_2O$ salts upon the framework decomposition (Fig. 3, Fig. S21 and S23, ESI†).

This finding shows that the drug release was triggered not only by the side ligand exchange but also by the framework decomposition, explaining the faster drug release at pH 6 compared to the drug release at pH 7.4.

Cytotoxicity studies

When intending to use nanoparticles as drug carriers, the cytotoxicity of the nanocarrier itself has to be evaluated and the cytotoxic effects of the original drug (here arsenic trioxide) have to be compared with those in the nanoparticle formulation (here MFU-4l-OAs(OH)$_2$).

The arsenic release studies revealed that MFU-4l-OAs(OH)$_2$ not only released the bound arsenic species but also degraded to release the ligand H_2-BTDD in acidic conditions. Therefore both, the unloaded nanoparticle MFU-4l and the H_2-BTDD

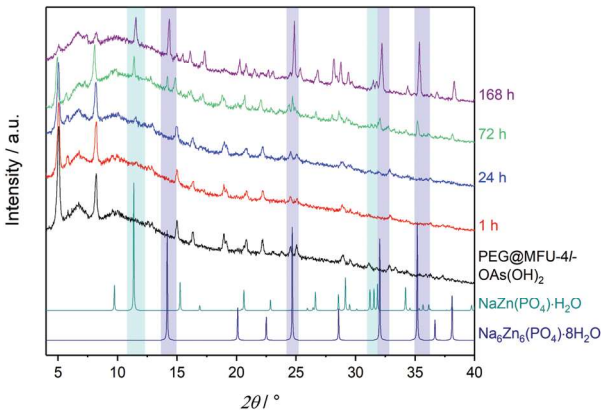

Fig. 3 Comparison of measured XRPD patterns of PEG@MFU-4l-OAs(OH)$_2$ (black), PEG@MFU-4l-OAs(OH)$_2$ after the arsenic release studies carried out at pH 7.4 for 1 h (red), 24 h (blue), 72 h (green) and 168 h (purple) and the calculated XRPD patterns of $NaZn(PO_4)\cdot H_2O$ (turquoise) and $Na_6Zn_6(PO_4)\cdot 8H_2O$ (dark blue).

ligand, were analysed with respect to their cytotoxic properties. For that purpose, non-tumorous control cell lines and different ATRT cell lines were incubated with five different concentrations of MFU-4l and H_2-BTDD for up to 72 h (Fig. 4). The administered concentrations of MFU-4l and H_2-BTDD were calculated with respect to the amount of these molecules, which was found in the arsenic loaded nanoparticles (equalling a concentration range of 0.0132–132 μM arsenic trioxide).

In the two control cell lines, MFU-4l reduced the cell viability: in case of the fibroblasts for concentrations of MFU-4l $\geq$ 0.8 mg L^{-1} after 24 h and 72 h (Fig. 4a), which would equal to an arsenic trioxide concentration of 1.32 μM, and in case of LLC-PK1 for concentrations $\geq$ 0.08 mg L^{-1} (only after 72 h, Fig. S24, ESI†), which would equal to an arsenic trioxide concentration of 0.132 μM. In ATRT cell lines (BT12, BT16, CHLA-02 and 311-FHTC), MFU-4l showed no significant cytotoxic effect (Fig. S24, ESI†), even after 72 h in the highest concentration. The cytotoxic effect of MFU-4l on normal tissue, represented in the *in vitro* study by the non-tumorous cell lines fibroblasts and LLC-PK1, was visible at lower doses in the range of the IC_{50} values (Table 2), albeit leading to a maximum decrease of cell viability of <25% (fibroblasts) and <35% (LLC-PK1), respectively. Further *in vivo* studies will elucidate if this effect is also seen in living organisms.

Table 2 Half-maximal inhibitory concentrations (IC_{50} values) after 72 h for arsenic trioxide and MFU-4l-OAs(OH)$_2$ treatment of different ATRT cell lines

	IC_{50} value [μM] after 72 h	
ATRT cell line	Arsenic trioxide	MFU-4l-OAs(OH)$_2$
BT12	1.4	1.5
BT16	6.1	8.9
CHLA-02	0.9	2.5
311-FHTC	7.1	7.5

Only at concentrations of $\geq$3.75 mg L^{-1}, which would equal to an arsenic trioxide concentration of 13.2 μM, H_2-BTDD showed a significant effect on the cell viability of fibroblasts (Fig. 4b) and BT16 cells (Fig. S25, ESI†), while there was no cytotoxic effect on BT12 cells (Fig. S25, ESI†). Compared to the IC_{50} values of tumour cell lines after 72 h (Table 2), H_2-BTDD exhibited a noteworthy cytotoxic effect only at concentrations higher than needed to bisect the cell viability in ATRT cell lines.

In the next step, it is of interest to compare the cytotoxic effects of arsenic trioxide (ATO) with those of MFU-4l-OAs(OH)$_2$. We therefore incubated ATRT cell lines with different concentrations of free arsenic trioxide and MFU-4l-OAs(OH)$_2$ for 72 h and assessed the cell viability *via* MTT assay. The results showed that both reduced the cell viability of ATRT cells *in vitro* (Fig. 5). The cytotoxic effect was cell-line as well as dose-dependent, with IC_{50} values ranging from 0.9 to 8.9 μM (Table 2). BT12 (Fig. 5a) and CHLA-02 cells (Fig. 5c) exhibited greater sensitivity towards arsenic trioxide and MFU-4l-OAs(OH)$_2$ than BT16 (Fig. 5b) and 311-FHTC (Fig. 5d) cells. Of note is that the cytotoxic effect of MFU-4l-OAs(OH)$_2$ was equal or lower than that of free arsenic trioxide, suggesting that the nanoparticle formulation did not add cytotoxicity, but rather acted as a neutral or slightly cytotoxicity attenuating cargo.

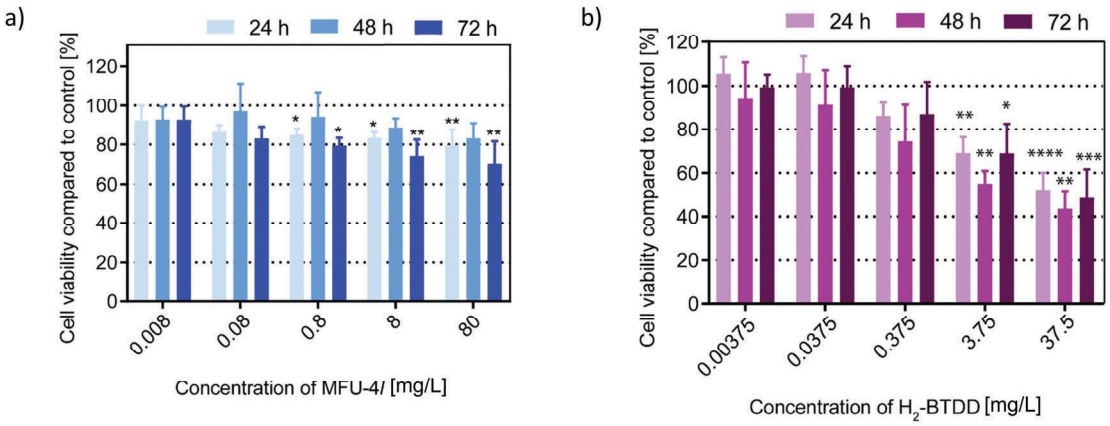

Fig. 4 Cell viability of fibroblasts after 24 h, 48 h and 72 h incubation with different concentrations of MFU-4l (a) and H_2-BTDD (b). Data are presented as mean ± standard deviation ($n \geq 3$) (ANOVA one-way, * indicates $p \leq 0.05$, ** $p \leq 0.01$, **** $p \leq 0.0001$).

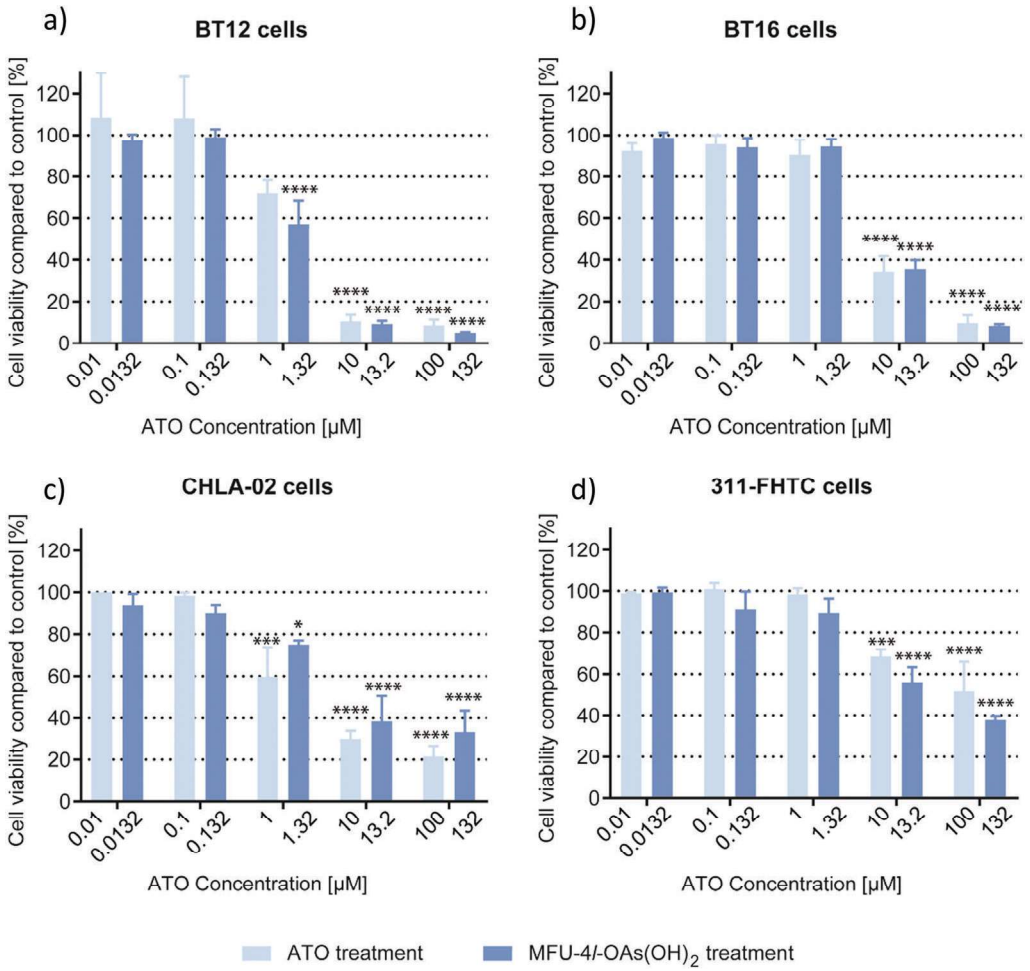

Fig. 5 Cell viability of different ATRT cell lines after 72 h incubation with different concentrations of ATO and MFU-4l-OAs(OH)$_2$. Data are presented as mean ± standard deviation ($n \geq 3$) (ANOVA one-way, * indicates $p \leq 0.05$, ** $p \leq 0.01$, *** $p \leq 0.001$, **** $p \leq 0.0001$).

Experimental

Materials and methods

All reagents were of analytical grade and used as received from commercial suppliers, except for bis(1*H*-1,2,3-triazolo[4,5-*b*],[4′,5′-*i*])dibenzo[1,4]dioxin which was prepared according to a previously published procedure.[28] Fourier transform infrared (FTIR) spectra were recorded in the range of 400–4000 cm^{-1} on a Bruker Equinox 55 FT-IR spectrometer equipped with an ATR unit. Thermogravimetric analysis (TGA) was measured on a TA Instruments Q500 device in a temperature range of 25–650 °C under a nitrogen atmosphere at a heating grade of 10 K min^{-1}. X-ray powder diffraction data were collected in the 4–40° 2θ range using a Seifert XRD 3003 TT powder diffractometer with a Meteor1D detector operating at room temperature using Cu $K_{\alpha 1}$ radiation (λ = 1.54187). Variable temperature X-ray powder diffraction (VT XRPD) were measured under nitrogen atmosphere with an Empyrean (PANalytical) diffractometer equipped with a Bragg–Brentano HD mirror, a PICcel3D 2 × 2 detector and a Cryo & humidity Chamber CHC plus+ (Anton Paar). The temperature program included a heating rate of 10 °C min^{-1} and then 10 min isothermal between the measurements. TEM micrographs were recorded on a JEM 2100F microscope (JEOL) with a FEG electron source operated at 200 kV. Samples were prepared by depositing a drop of the crystalline products dispersed in ethanol onto carbon-coated copper grids (200 mesh) and dried in air. Dynamic light scattering (DLS) measurements were carried out using a Brookhaven 90Plus Nanoparticle Size Analyzer. The elemental composition of solid samples was determined by energy dispersive X-ray spectroscopy (EDX) with the Philips XL 30 FEG with a EDAX SiLi detector, while liquid samples were analysed by ICP-OES with the Vista MPX of VARIAN with arsenic and zinc standard solution of 10 ppm and 20 ppm. Argon adsorption isotherms were measured with a Quantachrome Autosorb-I ASI-CP-8 instrument. The measurements were performed at 77.3 K in the range of $5.00 \times 10^{-5} \leq p/p_0 \leq 1.00$. Cells were cultivated in a Heracell™ 150i CO_2 incubator (Thermo Scientific). MTT assay was analysed using a Multiskan Ascent Microplate Reader (Thermo Electron Corporation).

Synthesis of MFU-4l nanoparticles $[Zn_5Cl_4(BTDD)_3]_n$

Bis(1*H*-1,2,3-triazolo[4,5-*b*],[4′,5′-*i*])dibenzo[1,4]dioxin (H_2-BTDD, 200 mg, 0.757 mmol) was dispersed in dimethylformamide (200 mL) in a 1 L round bottom flask and the mixture was

heated at 145 °C for 20 minutes in order to dissolve the ligand. Upon cooling down to 80 °C, 200 mL of a 0.076 M ethanolic solution of zinc chloride were added and the reaction mixture was kept at 80 °C for further 20 min with stirring. The product was first isolated by a centrifuge, then soaked in dimethylformamide (15 mL) overnight and washed with methanol twice (2 × 5 mL). To remove any solvent residues from the pores, the solid was dried at 160 °C under high vacuum for 15 h. By this method, 270 mg of MFU-4l nanoparticles (98% based on ligand) were prepared. The final material was appropriately characterised by XRPD, IR, TGA, TEM, SEM-EDX and adsorption analysis.

Drug loading

A methanolic solution of $[(CH_3)_4N]H_2AsO_3$ (0.1 M) was prepared by mixing As_2O_3 (98.92 mg, 0.5 mmol) and tetramethylammonium hydroxide (a 0.28 M methanolic solution, 3.51 mL) in a 10 mL volumetric flask and diluting with methanol to a total volume of 10 mL. 250 mg of MFU-4l nanoparticles were dispersed in 25 mL of the 0.1 M methanolic solution of $[(CH_3)_4N]H_2AsO_3$ for 30 min, washed with methanol (2 × 10 mL) and dried at 100 °C at ambient pressure. The drug loaded material [MFU-4l-OAs(OH)$_2$] was characterised by XRPD, IR, TGA, TEM, SEM-EDX, ICP-OES and adsorption analysis.

Coating drug loaded nanoparticles with polyethylene glycol

100 mg of MFU-4l-OAs(OH)$_2$ were dispersed in 10 mL of a 1.6 mM methanolic solution of polyethylene glycol (PEG 6000) and kept at room temperature. After 30 minutes the sample [PEG@MFU-4l-OAs(OH)$_2$] was collected by centrifuge, washed with methanol (3 × 5 mL) and dried under ambient pressure at room temperature. The material was characterised by XRPD, IR, TGA, SEM-EDX and ICP-OES.

Drug release

10 mg of drug loaded MFU-4l nanoparticles [MFU-4l-OAs(OH)$_2$] were dispersed in 10 mL of a 0.01 M phosphate buffer at pH 7.4 or at pH 6. At a certain period of time (30 min, 1 h, 4 h, 6 h, 24 h, 72 h and 168 h), 1 mL of the solution was removed for analysis and replaced by 1 mL of a fresh phosphate buffer solution. The amount of arsenic and zinc in the taken 1 mL sample was determined by ICP-OES analysis. The arsenic-release studies were done in triplicates, data are presented as mean ± standard deviation. To study the MOF stability, 10 mg of drug loaded MFU-4l nanoparticles [MFU-4l-OAs(OH)$_2$] were dispersed in 10 mL of a 0.01 M phosphate buffer at pH 7.4 or at pH 6. At a certain period of time (1 h, 24 h, 72 h and 168 h), the solid was isolated, washed twice with water and dried at 100 °C for 3 h. They were analysed with XRPD, IR and TGA.

Cell culture

BT12 cells (received as a gift from Marc Remke, University of Düsseldorf, Germany), BT16 cells (received as a gift from Martin Hasselblatt, University of Münster, Germany), ATRT-311FHTC cells (obtained from the Olson Lab, Fred Hutchinson Cancer Research Center, Seattle, USA) and ATRT-CHLA-02 cells (obtained from the American Tissue Culture Collection ATCC, Manassas, VA, USA) were grown in suspension and cultured with DMEM/F12-Medium supplemented with 2% B27 supplement, 1% N_2 supplement, 1% penicillin and streptomycin, 20 ng mL^{-1} EGF and 20 g mL^{-1} FGF. Fibroblasts (received as a gift from Niki Loges, University of Münster, Germany) and LLC-PK1 cells (received as a gift from Giuliano Ciarimboli, University of Münster, Germany) were grown adherently and cultured in DMEM – high glucose-medium supplemented with 20% FBS and 1% penicillin and streptomycin. All cells were cultured in 5% CO_2 at 37 °C. The identity of all cell lines was confirmed by STR-PCR.

Cytotoxicity studies

Cytotoxicity was evaluated *via* MTT assay, a well-established cell viability test.[40] Cells were seeded in a 96-well plate at a density of 750 (LLC-PK1), 2.000 (BT16), 3.000 (BT12), 4.000 (CHLA-02, fibroblasts) or 7.000 (311FHTC) cells per well. After 24 h, the cells were treated with increasing concentrations of MFU-4l, H_2-BTDD, MFU-4l-OAs(OH)$_2$ and ATO and incubated for up to 72 h. On the day of the measurement, 10 μL of the MTT reagent per well were added. Viable cells converted the tetrazolium dye MTT (3-(4,5-dimethylthiazol-2-yl)-2,5-diphenyltetrazolium bromide) into an insoluble, purple-coloured formazan dye. After 3.5 h incubation time, formazan crystals were broken by resuspension with 100 μL isopropanol + 0.04 M HCl per well. The absorbance was measured with a Multiskan Ascent Microplate Reader at a wavelength of 570 nm and a reference wavelength of 630 nm. Data was analysed using GraphPad Prism software version 7.03.

Statistical analysis

Cytotoxicity studies were done in biological triplicates, data are presented as mean ± standard deviation. The results were analysed by ANOVA one-way test. Statistical significance was assumed for $p \leq 0.05$. Single asterisk denotes $p \leq 0.05$, double asterisk denote $p \leq 0.01$, triple asterisks denote $p \leq 0.001$ and four asterisks denote $p \leq 0.0001$. IC_{50} values were calculated *via* non-linear regression analysis. GraphPad Prism 7.03 software was used for all statistical analysis.

Conclusions

In summary, nanoparticles of a metal–organic framework MFU-4l were successfully synthesized, functionalized with $H_2AsO_3^-$ anions *via* a side ligand exchange and their *in vitro* cytotoxicity was evaluated by MTT assay. Our studies showed that it was possible to exchange more than 86% of chloride anions of MFU-4l by $H_2AsO_3^-$. The prepared arsenic loaded MFU-4l nanoparticles were further coated with PEG 6000 and the arsenic release from the non-coated and coated samples was analysed in a phosphate buffered saline at pH 6 and 7.4. The drug release from the non-coated samples was high in the first few hours but could be significantly slowed down by the coating. Both, MFU-4l-OAs(OH)$_2$ and PEG@MFU-4l-OAs(OH)$_2$, reached almost complete release after 24 h and

showed a pH dependence with an enhanced arsenic release at lower pH. The characterization of the MOF after the release studies revealed that MFU-4l tended to exchange the $H_2AsO_3^-$ ions rapidly by coexisting anions such as most notably HPO_4^{2-} anions. Moreover, the framework partially decomposed, especially at lower pH values, which also accelerated the arsenic release. The cytotoxicity studies showed that MFU-4l-OAs$(OH)_2$ had similar effects on cancer cell lines as free arsenic trioxide and suggested that neither the carrier MFU-4l nor the free ligand H_2-BTDD caused critical harm for the tested cell cultures. Further *in vitro* cell penetration and *in vivo* studies will be necessary to evaluate the effects of nanoparticle-bound arsenic in comparison to free arsenic trioxide in cell cultures and mammals. Based on the example of MFU-4l reported here, we showed that metal–organic framework nanoparticles could be promising candidates for drug delivery of arsenic trioxide. In the near future we plan to test also other MOFs, including the cationic Fe-MIL MOFs, as carriers of arsenic trioxide species.

Conflicts of interest

There are no conflicts to declare.

Acknowledgements

Financial support by the Else Kröner-Fresenius Foundation (project no. 2016_A181) is gratefully acknowledged. We thank A. Kalytta-Mewes (Institute of Physics, University of Augsburg) for recording the VT XRPD measurement.

References

1 A. M. Stacy, J. A. Coonrod and J. Claesgens, Toxins, *Chemical reactions and stoichiometry*, Key Curriculum Press, Emeryville, CA, 2004, unit 4.
2 E. P. Swindell, P. L. Hankins, H. Chen, D. U. Miodragović and T. V. O'Halloran, *Inorg. Chem.*, 2013, **52**, 12292–12304.
3 European Medical Agency (EMA), Trisenox EMEA/H/C000388/II/0058 assessment report, 2016.
4 K. Kerl, N. Moreno, T. Holsten, J. Ahlfeld, J. Mertins, M. Hotfilder, M. Kool, K. Bartelheim, S. Schleicher, R. Handgretinger, U. Schüller, M. Meisterernst and M. C. Frühwald, *Int. J. Cancer*, 2014, **135**, 989–995.
5 A. Biswas, L. Kashyap, A. Kakkar, C. Sarkar and P. K. Julka, *Cancer Manage. Res.*, 2016, **8**, 115–125.
6 K. F. Ginn and A. Gajjar, *Front. Oncol.*, 2012, **2**, 114.
7 P. R. Subbarayan and B. Ardalan, *J. Gastrointest. Cancer*, 2014, **45**, 363–371.
8 A. Akhtar, S. Xiaoyan Wang, L. Ghali, C. Bell and X. Wen, *J. Biomed. Res.*, 2017, **31**, 177–188.
9 W. H. de Jong and P. J. A. Borm, *Int. J. Nanomed.*, 2008, **3**, 133–149.
10 A. Subastri, V. Arun, P. Sharma, E. Preedia Babu, A. Suyavaran, S. Nithyananthan, G. M. Alshammari, B. Aristatile, V. Dharuman and C. Thirunavukkarasu, *Chem.-Biol. Interact.*, 2017, DOI: 10.1016/j.cbi.2017.12.025 [Epub ahead of print].
11 O. M. Yaghi, M. O'Keeffe, N. W. Ockwig, H. K. Chae, M. Eddaoudi and J. Kim, *Nature*, 2003, **423**, 705–714.
12 N. Stock and S. Biswas, *Chem. Rev.*, 2012, **112**, 933–969.
13 O. K. Farha, I. Eryazici, N. C. Jeong, B. G. Hauser, C. E. Wilmer, A. A. Sarjeant, R. Q. Snurr, S. T. Nguyen, A. Ö. Yazaydın and J. T. Hupp, *J. Am. Chem. Soc.*, 2012, **134**, 15016–15021.
14 H. Li, K. Wang, Y. Sun, C. T. Lollar, J. Li and H.-C. Zhou, *Mater. Today*, 2018, **21**, 108–121.
15 L. Jiao, Y. Wang, H.-L. Jiang and Q. Xu, *Adv. Mater.*, 2018, **30**, 1703663.
16 L. Zhu, X.-Q. Liu, H.-L. Jiang and L.-B. Sun, *Chem. Rev.*, 2017, **117**, 8129–8176.
17 L. Liu, Y. Zhou, S. Liu and M. Xu, *ChemElectroChem*, 2018, **5**, 6–19.
18 L. E. Kreno, K. Leong, O. K. Farha, M. Allendorf, R. P. van Duyne and J. T. Hupp, *Chem. Rev.*, 2012, **112**, 1105–1125.
19 G. Maurin, C. Serre, A. Cooper and G. Ferey, *Chem. Soc. Rev.*, 2017, **46**, 3104–3107.
20 K. Lu, T. Aung, N. Guo, R. Weichselbaum and W. Lin, *Adv. Mater.*, 2018, 1707634.
21 T. Simon-Yarza, A. Mielcarek, P. Couvreur and C. Serre, *Adv. Mater.*, 2018, 1707365.
22 M. Giménez-Marqués, T. Hidalgo, C. Serre and P. Horcajada, *Coord. Chem. Rev.*, 2016, **307**, 342–360.
23 L. Wang, M. Zheng and Z. Xie, *J. Mater. Chem. B*, 2018, **6**, 707–717.
24 P. Horcajada, C. Serre, G. Maurin, N. A. Ramsahye, F. Balas, M. Vallet-Regí, M. Sebban, F. Taulelle and G. Férey, *J. Am. Chem. Soc.*, 2008, **130**, 6774–6780.
25 J. An, S. J. Geib and N. L. Rosi, *J. Am. Chem. Soc.*, 2009, **131**, 8376–8377.
26 P. Horcajada, C. Serre, M. Vallet-Regí, M. Sebban, F. Taulelle and G. Férey, *Angew. Chem., Int. Ed.*, 2006, **45**, 5974–5978.
27 V. Agostoni, P. Horcajada, M. Noiray, M. Malanga, A. Aykaç, L. Jicsinszky, A. Vargas-Berenguel, N. Semiramoth, S. Daoud-Mahammed, V. Nicolas, C. Martineau, F. Taulelle, J. Vigneron, A. Etcheberry, C. Serre and R. Gref, *Sci. Rep.*, 2015, **5**, 7925.
28 D. Denysenko, M. Grzywa, M. Tonigold, B. Streppel, I. Krkljus, M. Hirscher, E. Mugnaioli, U. Kolb, J. Hanss and D. Volkmer, *Chem. – Eur. J.*, 2011, **17**, 1837–1848.
29 D. Denysenko, J. Jelic, K. Reuter and D. Volkmer, *Chem. – Eur. J.*, 2015, **21**, 8188–8199.
30 D. Denysenko, M. Grzywa, J. Jelic, K. Reuter and D. Volkmer, *Angew. Chem., Int. Ed.*, 2014, **53**, 5832–5836.
31 H. Bunzen, M. Grzywa, M. Hambach, S. Spirkl and D. Volkmer, *Cryst. Growth Des.*, 2016, **16**, 3190–3197.
32 T. M. Loehr and R. A. Plane, *Inorg. Chem.*, 1968, **7**, 1708–1714.
33 L. Sarkisov and A. Harrison, *Mol. Simul.*, 2011, **37**, 1248–1257.
34 P. I. Ravikovitch and A. V. Neimark, *Colloids Surf., A*, 2001, **187–188**, 11–21.

35 J. Jagiello and M. Thommes, *Carbon*, 2004, **42**, 1227–1232.
36 *Developing solid oral dosage forms. Pharmaceutical theory & practice*, ed. G. G. Z. Zhang, L. X. Yu, R. V. Mantri, Y. Qiu and Y. Chen, Academic Press, Amsterdam, 2017.
37 J. Tao, Z. Tan, L. Diao, Z. Ji, J. Zhu, W. Chen and Y. Hu, *RSC Adv.*, 2018, **8**, 21735–21744.
38 V. Balamurali, T. M. Pramodkuma, N. Srujana, M. P. Venkatesh, N. V. Gupta, K. L. Krishna and H. V. Gangadhara, *Am. J. Drug Discovery Dev.*, 2011, **1**, 24–48.
39 C.-Y. Sun, C. Qin, X.-L. Wang, G.-S. Yang, K.-Z. Shao, Y.-Q. Lan, Z.-M. Su, P. Huang, C.-G. Wang and E.-B. Wang, *Dalton Trans.*, 2012, **41**, 6906–6909.
40 T. Mosmann, *J. Immunol. Methods*, 1983, **65**, 55–63.